ARTICLES
PUBLISHED ONLINE: 16 MAY 2010 | DOI: 10.1038/NCHEM.660

nature chemistry

Triggering N_2 uptake via redox-induced expulsion of coordinated NH_3 and N_2 silylation at trigonal bipyramidal iron

Yunho Lee, Neal P. Mankad and Jonas C. Peters*†

The biological reduction of N_2 to give NH_3 may occur by one of two predominant pathways in which nitrogenous N_xH_y intermediates, including hydrazine (N_2H_4), diazene (N_2H_2), nitride (N^{3-}) and imide (NH^{2-}), may be involved. To test the validity of hypotheses on iron's direct role in the stepwise reduction of N_2, model systems for iron are needed. Such systems can test the chemical compatibility of iron with various proposed N_xH_y intermediates and the reactivity patterns of such species. Here we describe a trigonal bipyramidal Si(*o*-$C_6H_4PR_2)_3$Fe–L scaffold (R = Ph or *i*-Pr) in which the apical site is occupied by nitrogenous ligands such as N_2, N_2H_4, NH_3 and N_2R. The system accommodates terminally bound N_2 in the three formal oxidation states (iron(0), +1 and +2). N_2 uptake is demonstrated by the displacement of its reduction partners NH_3 and N_2H_4, and N_2 functionalizaton is illustrated by electrophilic silylation.

Recent work by our group and several others targeted the synthesis of a variety of Fe–N_xH_y small-molecule model complexes, motivated by two goals[1–4]. First and foremost is the desire to develop synthetic catalysts with modes of action that might relate to, or at least stimulate hypotheses concerning, the manner by which biological nitrogenases reduce N_2 (refs 5–8). Second, the need to build a library of Fe–N_xH_y model complexes as a point of reference to be better able to interpret the spectroscopic data obtained recently for proposed intermediates of the N_2-ase cofactor. Of specific interest to us are Fe–N_xH_y complexes with iron centres that reside in geometries that are either four- or five-coordinate and feature local three-fold symmetry in which the N_xH_y can be viewed as occupying an axial site[9,10]. Such geometries may be relevant to some, if not all, of the intermediates of iron-bound N_2 reduction cycles, as suggested elsewhere[5,11].

With these goals in mind we recently began to work with monoanionic tetradentate trisphosphinosilyl SiP^R_3 ligands (SiP^R_3 represents $(Si(o\text{-}C_6H_4PR_2)_3)^-$, R = Ph or *i*-Pr) that accommodate mononuclear, open-shell, five-coordinate iron(II) and iron(I) species with a proclivity towards binding N_2 in the axial site of a trigonal bipyramid (TBP) at a position that is *trans* to the silyl anchor[12,13]. Preliminary reactivity data established that protonation of N_2 can occur in modest yield to liberate N_2H_4 (ref. 12). Hence, it became of interest to target hydrazine complexes and other open-shell iron complexes that feature nitrogenous ligands in the axial site. Established herein is that the (SiP^R_3)Fe template binds N_2 axially *trans* to the silyl anchor in three distinct oxidation states that can be represented formally as iron(0), +1 and +2. To our knowledge, no previously established transition-metal system had been characterized that could accommodate terminal N_2 ligation across three oxidation states; however, an independent and related study characterizing terminally bonded Co–N_2 complexes across three states of oxidation, two of which have been structurally characterized, appeared while this manuscript was in press[14]. In addition, the recycling of Fe(II)–NH_3 and Fe(II)–N_2H_4 complexes to give Fe(I)–N_2 with expulsion of NH_3 is illustrated. This transformation is of interest as a key step of a hypothetical catalyst cycle in which the iron(I) oxidation state is used to trigger N_2 uptake and NH_3 release. Finally, we show also that it is possible to silylate directly the coordinated N_2 ligand to produce Fe–N_2SiR_3 products that appear to be far more stable than their Fe–N_2H counterparts. This reactivity pattern, which is well established for certain molybdenum systems, is not well known for iron[15]. In sum, these chemical properties add motivation to the search for a molecular N_2-reduction catalyst that uses iron as the redox active centre to facilitate N_2 binding and reduction.

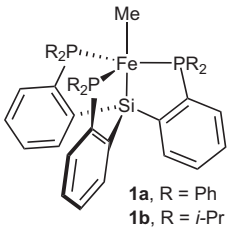

The most convenient means of entry into the chemistry described herein proceeds through the iron(II) methyl complexes $(SiP^{Ph}_3)Fe(CH_3)$ (**1a**) and $(SiP^{i\text{-}Pr}_3)Fe(CH_3)$ (**1b**). CH_3MgCl was added to a mixture of ferrous chloride and the corresponding silane $H(SiP^R_3)$ in tetrahydrofuran (THF) at −78 °C, and then stirred overnight at room temperature, to afford the red ($S = 1$ spin state) methyl complexes **1a** and **1b** in good yield. Although these species can be isolated in relatively pure form, trace amounts of the $(SiP^R_3)Fe(N_2)$ complex were present typically because of the competitive reduction by CH_3MgCl. The solid-state structures of **1a** and **1b** were determined (see Supplementary Information for details) and showed nearly ideal TBP geometries at the iron centres ($\tau = 0.91$ for **1a** and 0.96 for **1b**, where $\tau = 0.00$ for a perfect square pyramid and $\tau = 1.00$ for a TBP geometry[16]). The solid-state structures are noteworthy in that the methyl ligands occupy axial sites *trans* to the silyl anchors (see Supplementary Information). Cyclic voltammetry (CV) of **1a** revealed two reversible redox waves, $E_{1/2} = -0.57$ and −2.3 V (Fe(III/II) and Fe(II/I), respectively, versus ferrocene/ferrocenium

Department of Chemistry, Massachusetts Institute of Technology, Cambridge MA 02139, USA; †Present address: Division of Chemistry and Chemical Engineering, California Institute of Technology, Pasadena, California 91125, USA. *e-mail: jpeters@caltech.edu

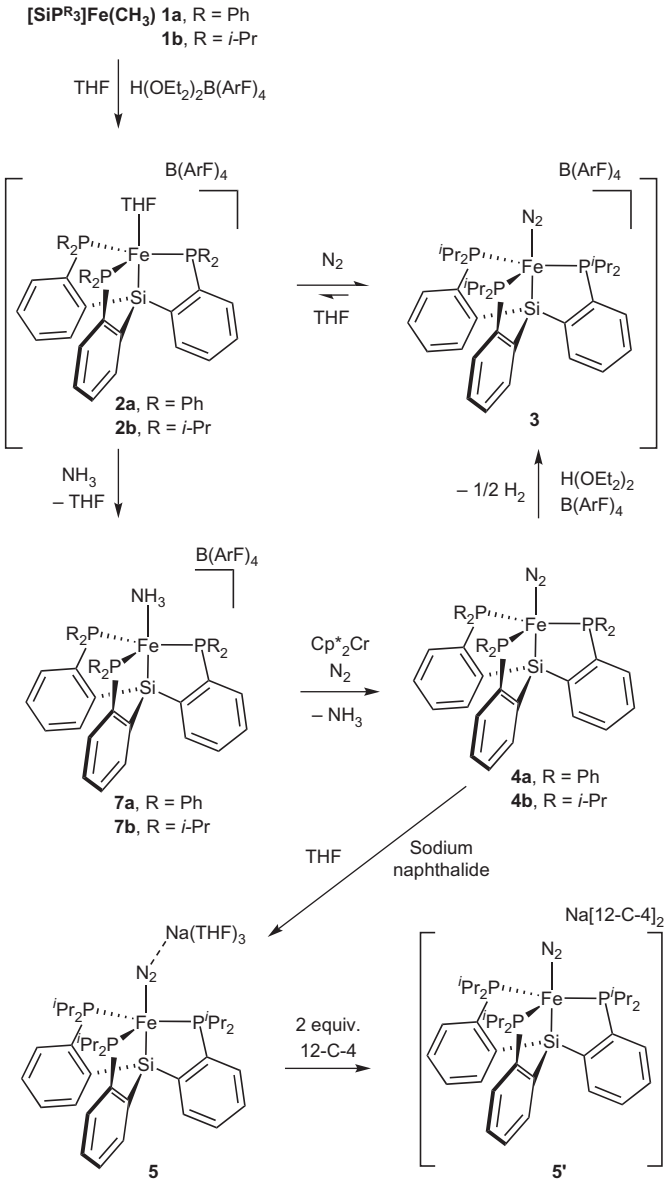

Figure 1 | Synthetic scheme for the generation of Fe-N_2^+, Fe-N_2 and Fe-N_2^- (3, 4b, 5 and 5′). Exposure of NH_3 to cationic Fe-THF$^+$ (**2a**, R = Ph or **3**, R = *i*-Pr) affords the NH_3 complexes **7a** or **7b**. On addition of Cp^*_2Cr (decamethylchromocene), N_2 uptake generates Fe-N_2 (**4a** or **4b**) with the quantitative release of NH_3. Sodium naphthalide reduction of **4b** generates Fe-N_2^- (**5** and **5′**).

($FeCp_2/FeCp_2^+$); see Supplementary Information). Corresponding redox events for the isopropyl derivative **1b** were shifted cathodically by ~300 mV.

Synthesis and characterization of Fe–N_2, Fe–N_2^+ and Fe–N_2^-. Exposure of the methyl complexes to acid sources selectively released methane. In THF solvent with $H(OEt_2)_2(B(ArF)_4)$ as the added acid ($B(ArF)_4 = B(3,5\text{-}(CF_3)_2C_6H_3)_4$), **1a** was protonated to generate the cationic THF adduct $\{(SiP^{Ph}_3)Fe(II)(THF)\}\{B(ArF)_4\}$ (**2a**). By contrast, exposure of the more electron-releasing species **1b** to $H(OEt_2)_2(B(ArF)_4)$ under nitrogen favoured the formation of the cationic nitrogen complex $\{(SiP^{i\text{-}Pr}_3)Fe(II)(N_2)\}\{B(ArF)_4\}$ (**3**) (Fig. 1), which in THF solution under an atmosphere of nitrogen dominated the THF-adduct species by a ratio of about 6:1, as determined by ultraviolet–visible analysis. Alternatively, **3** can be obtained as a blue powder by adding $H(OEt_2)_2(B(ArF)_4)$ to a benzene solution of the previously reported red N_2 adduct $(SiP^{i\text{-}Pr}_3)Fe(N_2)$ (**4b**) (ref. 13). Gas chromatography analysis confirmed H_2 as the by-product of the latter reaction (see Supplementary Information for details).

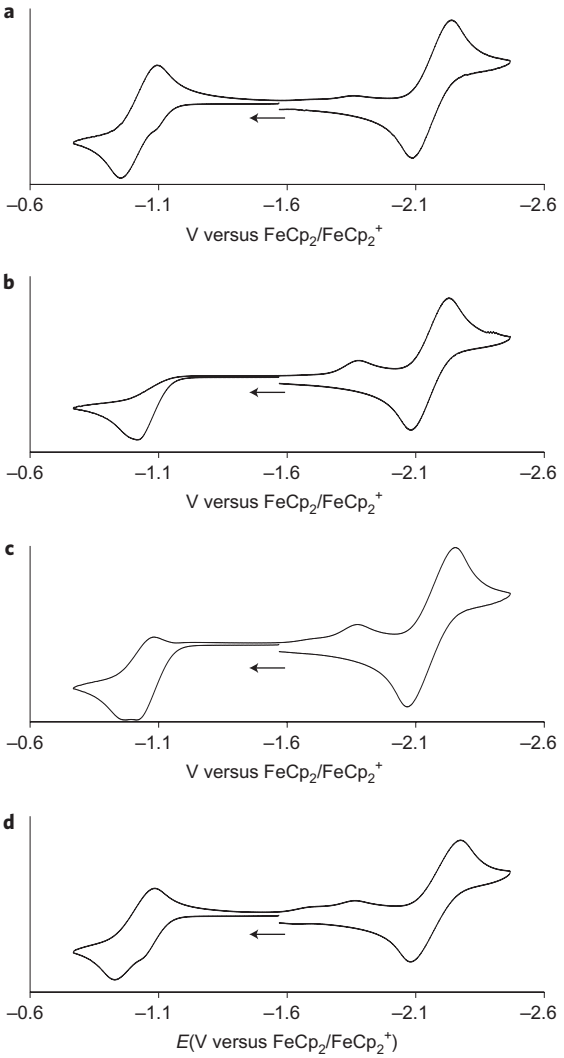

Figure 2 | CV behaviour of $(SiP^{i\text{-}Pr}_3)Fe(N_2)$ (4b). a–d, Under an N_2 atmosphere (**a**), after sparging the sample with argon for 30 s (**b**), after partial removal of argon under vacuum and re-exposure to an N_2 atmosphere (**c**) and after another vacuum-N_2 exposure cycle (**d**). Data collected in THF at 100 mV s^{-1} and 0.3 M $\{n\text{-}Bu_4\}\{PF_6\}$.

The presence of cationic $(SiP^{i\text{-}Pr}_3)Fe(N_2)^+$ species was gleaned by comparing the CV of the neutral N_2 adduct $(SiP^{i\text{-}Pr}_3)Fe(N_2)$ (**4b**) under a nitrogen or argon atmosphere in THF solution. Figure 2a shows the cyclic voltammogram of **4b** under a nitrogen atmosphere. Two prominent and reversible waves are present at about –1.0 V and –2.2 V versus $FeCp_2/FeCp_2^+$. These are assigned as the Fe–N_2/Fe–N_2^+ and Fe–N_2/Fe–N_2^- waves, respectively. The wave at –1.0 V shows a small shoulder on its negative side (–1.1 V) that we presume arises from the generation of Fe–THF$^+$ in addition to that of Fe–N_2^+ on oxidation. As the sample was scanned cathodically a small feature appeared at −1.9 V, which we presume results from the irreversible reduction of Fe–THF$^+$. Indeed, when **4b** was sparged for 30 seconds with argon (Fig. 2b) the oxidation wave at –1.0 V, which corresponds to the oxidation of Fe–N_2, was no longer reversible because oxidation leads to rapid loss of N_2. Accordingly, the peak at –1.9 V increased in intensity because the generation of Fe–THF$^+$ is favoured under argon. Re-admission of

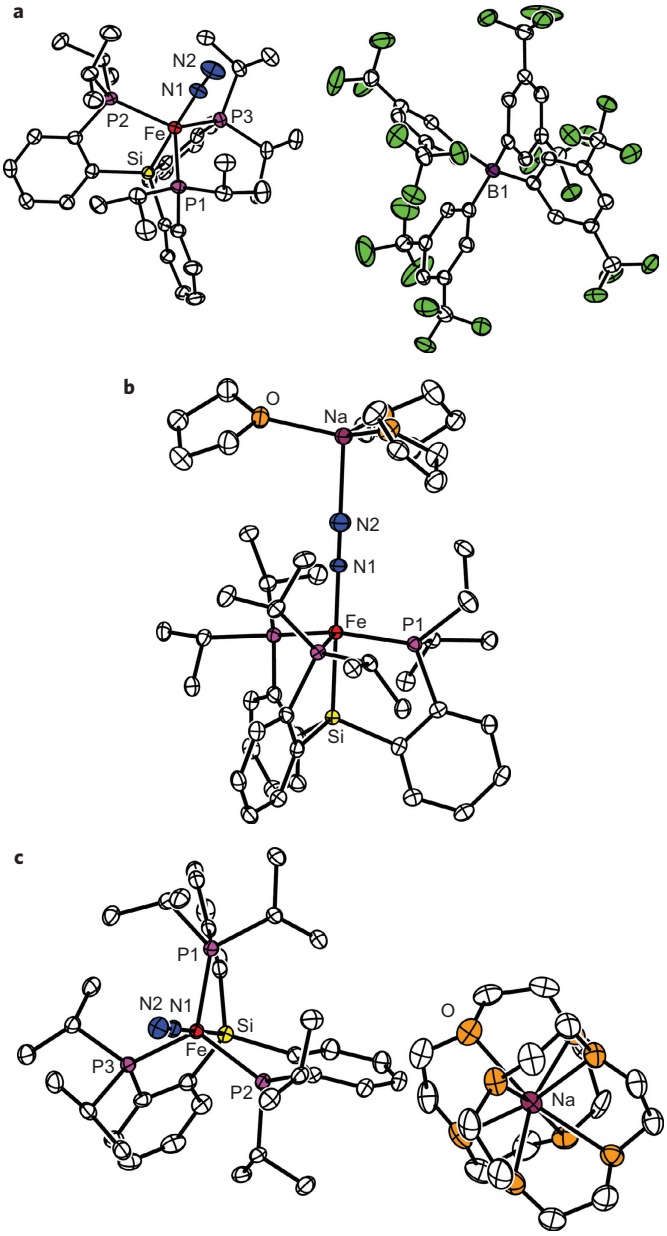

Figure 3 | Solid-state structures of 3, 5 and 5′. a, $\{(SiP^{i\text{-}Pr}_3)Fe(N_2)\}\{B(ArF)_4\}$ (**3**). **b**, $\{(SiP^{i\text{-}Pr}_3)Fe(N_2)\}\{Na(THF)_3\}$ (**5**). **c**, $\{(SiP^{i\text{-}Pr}_3)Fe(N_2)\}\{Na(12\text{-}C\text{-}4)_2\}$ (**5′**). All hydrogen atoms and molecules of co-crystallization are omitted for clarity. See Supplementary Information for complete details.

nitrogen into the solution after removal of most of the argon by rapid evacuation (Fig. 2c) gave rise to a partially recovered return wave at −1.0 V, which grew in intensity after thorough sparging with nitrogen (Fig. 2d) to provide a trace very similar to that observed initially (Fig. 2a), with the exception of a modest impurity that appears at about −1.7 V. One additional species to consider in the context of the assignments proposed concerns trigonal pyramidal $(SiP^{i\text{-}Pr}_3)Fe$. The N_2 ligand of **4b** is modestly labile and it could therefore be that some of the minor features in the CV traces shown in Fig. 2 arise from redox at such a four-coordinate $(SiP^{i\text{-}Pr}_3)Fe$ species, for example the wave at −1.9 V. Our preference to assign this wave to the reduction of $Fe\text{–}THF^+$ in part arises because when N_2 was removed (Fig. 2b) the solution colour (orange) was that of other five-coordinate and divalent $(SiP^{i\text{-}Pr}_3)Fe(L)^+$ species, for example the hydrazine adduct **6b** (see below).

We were gratified to find that the cationic complex **3** was sufficiently stable to be isolated and characterized. Its $S = 1$ spin state is comparable to that of its nearly isostructural $S = \frac{1}{2}$ relative **4b** (previously reported[12]). Reduction of **4b** by sodium naphthalide afforded the formally zerovalent congener $\{(SiP^{i\text{-}Pr}_3)Fe(N_2)\}\{Na(THF)_3\}$ (**5**). The addition of two equivalents of 12-crown-4 (12-C-4) to **5** encapsulated the Na^+ and provided terminally bonded $\{(SiP^{i\text{-}Pr}_3)Fe(N_2)\}\{Na(12\text{-}C\text{-}4)_2\}$ (**5′**). High-resolution crystal structures were obtained for **3**, **5** and **5′** to accompany that previously reported for **4b**. These structural data collectively afford the only such data available for a terminally bonded N_2 adduct of any transition metal in three distinct oxidation states (Fig. 3 and Table 1)[14]. Yandulov and Schrock reported that the trivalent molybednum dinitrogen adduct $((HIPTNCH_2CH_2)_3N)Mo(N_2)$ (HIPT = 3,5-(2,4,6-*i*-$Pr_3C_6H_2)_2C_6H_3$) showed electrochemically reversible waves assigned as $Mo\text{–}N_2^{+/0}$ and $Mo\text{–}N_2^{0/-}$, where the neutral and anionic derivatives were characterized structurally, the latter as a Mg adduct[17]. Key to this iron system is that the N_2 ligand remains in the site *trans* to the Si anchor in each state of oxidation, and the iron centre's geometry is preserved in the cationic, neutral and anionic species. Structural changes include a contraction of the Fe–N bond distance as the system was reduced successively, and a corresponding Fe–Si contraction on successive reduction (Table 1).

Synthesis and characterization of $Fe\text{–}NH_3^+$, $Fe\text{–}N_2H_4^+$ and $Fe\text{–}N_2H_3B(C_6F_5)_3$. The cationic THF and N_2 adducts are labile at the axial site *trans* to the silyl donor, and hence provide one pathway by N_2H_4 addition to the corresponding hydrazine-adduct derivatives $\{(SiP^{Ph}_3)Fe(II)(N_2H_4)\}\{B(ArF)_4\}$ ($\{$**6a**$\}\{B(ArF)_4\}$) and $\{(SiP^{i\text{-}Pr}_3)Fe(II)(N_2H_4)\}\{B(ArF)_4\}$ ($\{$**6b**$\}\{B(ArF)_4\}$), respectively. Alternatively, slow addition of the hydrazinium acid $N_2H_5CF_3SO_3$ to either **1a** or **1b** in THF generated dark-red solutions of $\{$**6a**$\}\{OTf\}$ and $\{$**6b**$\}\{OTf\}$ (OTf = trifluoromethanesulfonate), both of which could be isolated in >90% yield. Their $S = 1$ spin states ($\mu_{eff} = 2.79\ \mu_B$ for **6a** and $3.0\ \mu_B$ for **6b**) are consistent with TBP structures (Fig. 4), as confirmed by X-ray diffraction (XRD) analysis ($\tau = \sim 0.9$ for **6a** and 0.96 for **6b**). In each case their solid-state structures contain a hydrazine ligand η^1 coordinated to a five-coordinate iron centre in an axial site opposite the silyl anchor. For comparison, diamagnetic and six-coordinate η^2-hydrazine iron(II) complexes that utilize bidentate phosphine ligands have been reported[2,18,19]. As indicated in Fig. 4 for

Table 1 | N_2-adduct species 3, 4b, 5 and 5′.

	$\{FeN_2\}\{B(ArF)_4\}$ 3	Fe-$N_2^{\S}$ 4b	$\{FeN_2\}\{Na(THF)_3\}$ 5	$\{FeN_2\}\{Na(12\text{-}C\text{-}4)_2\}$ 5′
ν(N-N)* (cm^{-1})	2,143	2,003	1,891	1,920
N-N (Å)	1.091(3)	1.1245(2)	1.147(4)	1.132(4)
Fe-N (Å)	1.914(2)	1.8191(1)	1.763(3)	1.795(3)
Fe-Si (Å)	2.298(7)	2.2713(6)	2.2526(9)	2.236(1)
Si-Fe-N (°)	178.63(8)	178.73(5)	180.00(0)	179.8(1)
Colour† (nm (M^{-1} cm^{-1}))	Blue, 500 (270), 610 (145)	Red, 380 (3,500)	Purple, 510 (3,600)	Purple, 520 (3,800)
Spin state‡	3.3 BM, $S = 1$	2.2 BM, $S = \frac{1}{2}$	Diamagnetic	Diamagnetic

Physical parameters for the N_2-adduct species **3**, **4b**, **5** and **5′**. *KBr pellet. †THF solution. ‡Evans' method in THF-d_8 (**3**); §Updated X-ray data, structure originally reported[13] contains ~4% $(SiP^{i\text{-}Pr}_3)FeCl$.

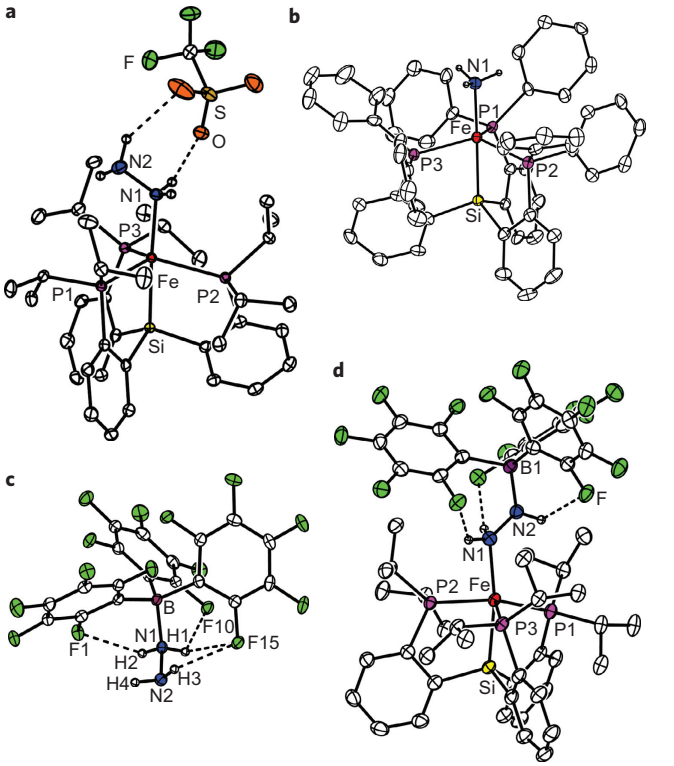

Figure 4 | Solid-state structures of {6b}{OTf}, 7a, $N_2H_4B(C_6F_5)_3$ and 9b. **a**, $\{(SiP^{i\text{-}Pr}{}_3)Fe(II)(N_2H_4)\}\{OTf\}$ ({**6b**}{OTf}). **b**, $\{(SiP^{Ph}{}_3)Fe(II)(NH_3)\}\{B(ArF)_4\}$ (**7a**). **c**, $N_2H_4B(C_6F_5)_3$. **d**, $(SiP^{i\text{-}Pr}{}_3)Fe(II)(N_2H_3B(C_6F_5)_3)$ (**9b**). Selected hydrogen atoms and the $(B(ArF)_4)$ anion of **7a** are omitted for clarity. See Supplementary Information for details.

{**6b**}{OTf}, the hydrazine moieties in {**6a**}{OTf} and {**6b**}{OTf} are hydrogen bonded to the triflate anions in the solid state, with average N–O distances of ~3 Å. In **6b**, the hydrogen atoms can be located in the difference map at an average distance of ~2 Å for N–H ··· O. The infrared spectra of these complexes contain N–H vibrations that show the presence of hydrogen bonds. These vibrations are broadened and shifted in solid-state spectra from those of their hydrazine derivatives with no hydrogen bonds, {**6a**}$\{B(ArF)_4\}$ and {**6b**}$\{B(ArF)_4\}$. Hydrazine adducts with a η^1-binding mode to five-coordinate metal complexes are not common[4,20–25]. To our knowledge, the only other example of such a species that shows approximate three-fold symmetry akin to that of **6a** and **6b** is a vanadium hydrazine complex supported by a tris(thiolate)amine ligand[26].

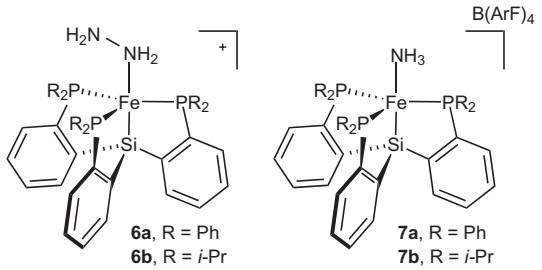

The hydrazine ligand is labile for both **6a** and **6b**, and binding of the triflate anion with the concomitant release of N_2H_4 was observed by NMR spectroscopy in C_6D_6. Lability at the apical site, although potentially useful for a catalytic system, is problematic with regard to attempts to generate an Fe(HN=NH) complex by oxidation of **6a** and **6b**. For instance, our attempts to oxidize these hydrazine complexes with $Pb(OAc)_4$ afforded mixtures of the neutral $\{(SiP^R{}_3)Fe(OTf)\}$ (ref. 13) and $\{(SiP^R{}_3)Fe(OAc)\}$ complexes (see Supplementary Information). Perhaps more interesting is that **6b** can be oxidized fully by 3,5-di-*t*-butyl-*o*-benzoquinone to give $\{(SiP^{i\text{-}Pr}{}_3)Fe(II)(N_2)\}^+$. (It is likely that the N_2 in the product derives from both the original N_2H_4 in the precursor and from atmospheric N_2 because of rapid ligand exchange.)

By analogy to the conversion of **6a** and **6b**, a THF solution of NH_3 reacts with either **2a** or **3** to give the cationic NH_3 adducts $\{(SiP^{Ph}{}_3)Fe(II)(NH_3)\}\{B(ArF)_4\}$ (**7a**) and $\{(SiP^{i\text{-}Pr}{}_3)Fe(II)(NH_3)\}\{B(ArF)_4\}$ (**7b**), respectively (Fig. 4). The NH_3 ligand is substitutionally labile and hence to obtain rigorously pure samples by thorough drying is a challenge: solvents in which the compounds dissolve (for example, THF) partially substitute the NH_3 ligand. Triplet **7b** ($\mu_{eff} = 3.27\ \mu_B$) was characterized structurally and, as for the hydrazine derivatives, features an NH_3 ligand in the apical site opposite the silyl donor. Although its structure (Fig. 4) is unremarkable, it underlines that the apical site of the $\{(SiP^{i\text{-}Pr}{}_3)Fe\}$ system can accommodate N_2 in the 0, +1 and +2 oxidation states, whereas NH_3 ligation appears accessible only in the +2 oxidation state. Indeed, when we tried to reduce either **7a** or **7b**, NH_3 was released quantitatively and the Fe(I)–N_2 adducts **4a** and **4b** were generated, respectively. The significance of this transformation lies in the ability to recycle Fe(I)–N_2 with the release of NH_3, key to the ultimate viability of a hypothetical Fe(I)–N_2 catalyst system to generate NH_3. Also, the reduction of the hydrazine adducts **6a** and **6b** led to facile generation of **4a** and **4b**, respectively. In these cases, both N_2H_4 and NH_3 were generated, as determined by vacuum transfer of the volatiles.

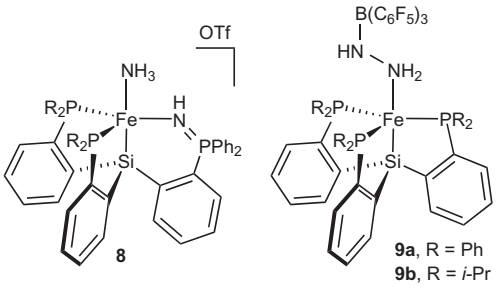

A rare N_xH_y ligand for iron that we sought within this system is the hydrazido ($N_2H_3^-$) ligand[3]. We reasoned that the hydrazine adducts **6a** and **6b** might afford access to such complexes through deprotonation. Although this did not turn out to be the case, the reaction that resulted is interesting. When a THF solution of {**6a**}{OTf} was exposed to a stoichiometric equivalent of N^1,N^1,N^8,N^8-tetramethylnaphthalene-1,8-diamine (proton sponge), a reaction ensued that afforded the paramagnetic NH_3-adduct complex $\{(Si(o\text{-}C_6H_4PPh_2)_2(o\text{-}C_6H_4P(=NH)Ph_2))Fe(NH_3)\}\{OTf\}$ (**8**), which was identified by XRD analysis. Its structure reveals that one arm of the $SiP^{Ph}{}_3$ ligand is oxidized to P(V) by formal insertion of NH into the Fe–P bond. The N–P bond distance in **8** of 1.5945(1) Å is very close to those of other reported N=P double bonds[27–32]. Infrared spectroscopy shows N–H vibrations at 3,339, 3,256 and 3,168 cm^{-1}. Complexes **6a** and **8** are hence structural isomers of one another and the role of the base thereby appears to be catalytic. The details of this reaction are, however, unclear and complicated by the presence of unidentified by-products.

Although the terminally bonded $N_2H_3^-$ ligand is elusive for these $\{(SiP_3)Fe\}$ systems, such a ligand can be generated in the presence of the Lewis-acid acceptor $B(C_6F_5)_3$. Thus, the addition of $(C_6F_5)BNH_2NH_2$ to **1a** or **1b** led to the formation of the neutral and zwitterionic iron(II) hydrazido-borane complexes $(SiP^{Ph}{}_3)Fe(II)(N_2H_3B(C_6F_5)_3)$ (**9a**) and $(SiP^{i\text{-}Pr}{}_3)Fe(II)(N_2H_3B(C_6F_5)_3)$ (**9b**) (Fig. 4). The hydrazine–borane adduct $N_2H_4B(C_6F_5)_3$ was synthesized from a 1:1 mixture of hydrazine and tris(pentafluorophenyl)borane in THF. Both **9a** and **9b** gave easily resolved ^{19}F NMR signals at −123, −157 and −162 ppm, despite their triplet ground

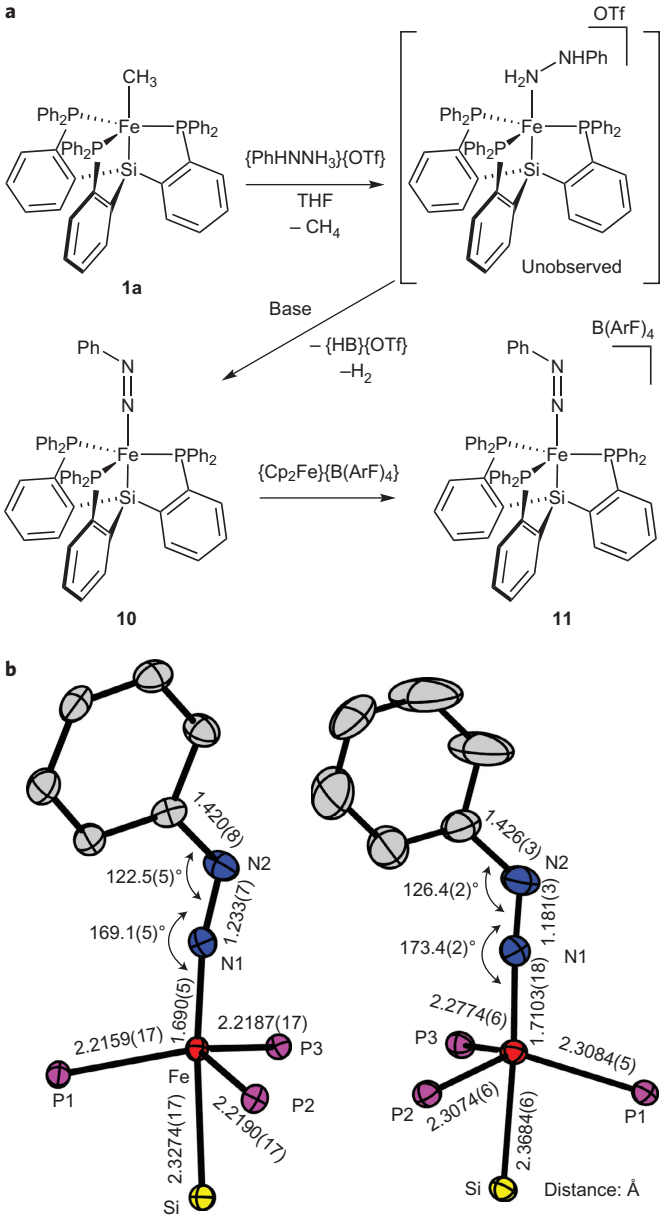

Figure 5 | Synthesis and characterization of 10 and 11. a, Synthetic scheme for the generation of $(SiP^{Ph}_3)Fe(II)(N_2C_6H_5)$ (**10**) and $\{(SiP^{Ph}_3)Fe(II)(N_2C_6H_5)\}\{B(C_6H_3(CF_3)_2)_4\}$ (**11**). **b**, Core-atom 50% probability ellipsoid representations of the solid-state structures of **10** and **11**.

states ($\mu_{eff} = 2.90\ \mu_B$ and $2.83\ \mu_B$). Solid-state crystal structures reveal η^1-bound hydrazido-borane ligands with the borane terminating the β-NH (see Fig. 4). To our knowledge, this ligand type is unique.

The B–N bonds (1.544(5) Å for **9a** and 1.553(3) Å for **9b**) are much shorter than that of the precursor $N_2H_4B(C_6F_5)_3$ (1.6316(19) Å). The N–N bond distances are 1.449(4) and 1.442(10) Å for **9a** and **9b**, respectively, which are slightly shorter than that in free $N_2H_4B(C_6F_5)_3$. Interestingly, hydrogen bonds between the hydrogen atoms of hydrazine (and hydrazido) and *ortho*-fluorine atoms of $B(C_6F_5)_3$ are exhibited in **9a** and **9b**, and also in the precursor $N_2H_4B(C_6F_5)_3$ (Fig. 4). In the literature these intramolecular N–H···F–C hydrogen bonds are relatively unusual examples of hydrogen bonding[33–37]. All hydrogen-bonded H-atoms can be located from the difference maps of the corresponding X-ray crystallographic data, and display distances in the H···F hydrogen bond range 2.158 ~ 2.356 Å.

Synthesis and characterization of Fe–N_2Ph and Fe–N_2SiMe_3. To attempt the synthesis of a monosubstituted hydrazido derivative, the methyl complex **1a** was exposed to phenylhydrazinium triflate (Fig. 5a). The reaction instead afforded a mixture of species presumed to contain paramagnetic $\{(SiP^{Ph}_3)Fe(NH_2–NHPh)\}\{OTf\}$ and $(SiP^{Ph}_3)Fe(OTf)$. In an attempt to isolate a well-defined Fe(II)(NH–NHPh) species the addition of base was tried. However, although the addition of base appeared to remove H^+ it also triggered the formal loss of H_2 to afford the phenyldiazenido complex $\{(SiP^{Ph}_3)Fe(N_2C_6H_5)\}$ (**10**, Fig. 5a). This is true for bases such as proton sponge and also for phenylhydrazine ($PhNH–NH_2$), which is necessarily present in solution. Dark-brown crystals of **10** were isolated from the reaction mixture in good yield (~70%), and infrared spectroscopy revealed an N–N vibration at 1,623 cm^{-1}. The solid-state crystal structure (Fig. 5b) confirms a η^1-phenyldiazenido ligand in an axial position *trans* to the silyl donor, with short N–N and Fe–N distances (1.233(7) and 1.690(5) Å), which reflects a multiple-bond character in each linkage. The N–N–C angle (122.5(5)°) establishes sp^2 hybridization at N_β. Diazenido **10** is structurally distinct because it has a diazenido ligand that occupies an axial position of a TBP geometry. For the few five-coordinate iron diazenido complexes that have been characterized structurally, the diazenido ligand occupies an equatorial site[38–41].

The reaction of $\{(SiP^{Ph}_3)Fe(THF)\}\{B(ArF)_4\}$ (**2a**) and phenyl hydrazine gave a red solution of $\{(SiP^{Ph}_3)Fe(NH_2–NHPh)\}^+$, with hydrazine-like ^{1}H-NMR signatures based on comparison with the spectra of **6a** and **6b**. N–H vibrations were observed at 3,346, 3,271 and 3,230 cm^{-1}. The red product was unstable and slowly converted into the NH_3 adduct **7a** at room temperature, presumably as a result of disproportionation of the iron-bound phenylhydrazine. The major organic product is aniline, as identified by ^{1}H-NMR spectroscopy and gas chromatography. Use of an excess of phenylhydrazine instead gave the inky black product $[(SiP^{Ph}_3)Fe(N_2C_6H_5)]^+$ (**11**). The same product was also obtained by the addition of $\{Cp_2Fe\}\{B(ArF)_4)\}$ to **10** in C_6D_6 solution. The N–N vibrational frequency (ν(N–N)) of **11** is 1,690 cm^{-1}, which reveals comparatively less back donation from iron to the N–N π^*-orbital than that for **10**. This is also supported by the solid-state structure of **11**, which shows a shorter N–N bond distance and a longer Fe–N bond distance than those for **10** (Fig. 5). Harder to explain is the curious lengthening of the Fe–P bond distances on oxidation of **10** to give **11**.

Our isolation of the phenyldiazenido complexes **10** and **11** motivated us to explore whether we might be able to prepare related diazenido complexes by direct functionalization of the iron-bound N_2 ligand in the neutral adduct complexes **4a** and **4b** or in the anion **5**. Whereas we showed previously that the N_2 ligand in **4a** can be protonated in modest yield to release hydrazine (46% in the presence of $CrCl_2$), to trap a derivatized N_2 ligand still bound to the iron centre has proved elusive for the phenyl-decorated $(SiP^{Ph}_3)Fe$ system. When $H(OEt_2)_2(B(ArF)_4)$ or CH_3OTf were added to **5** in THF at low temperature, thermally unstable and as yet uncharacterized species appeared that eventually decayed to the iron(I) N_2 adduct **4b**. At this stage we can only speculate as to the presence of Fe–N_2H and Fe–N_2Me intermediates. The use of silyl electrophiles has proved more fruitful with regard to the isolation of products. Thus, treatment of **5** with trimethylsilyl (TMS) chloride or TMSOTf in frozen THF followed by gradual warming of the solution afforded the desired dark-red diazenido complex $(SiP^{i\text{-}Pr}_3)Fe(N_2SiMe_3)$ (**12**) with concomitant salt elimination (Fig. 6). Complex **12** can also be generated directly from **4b** if Na–Hg amalgam is used as a reductant in the presence of TMSCl. The analogous complexes $(SiP^{i\text{-}Pr}_3)FeN_2Si^{i\text{-}Pr}_3)$ and $(SiP^{i\text{-}Pr}_3)Fe(N_2SiPh_3)$ were obtained using triisopropylsilyl-OTf and triphenylsilyl chloride, respectively. In contrast to its $S = 1$ relative **10**, diazenido **12** is diamagnetic. Two ^{29}Si-NMR resonances are present in the

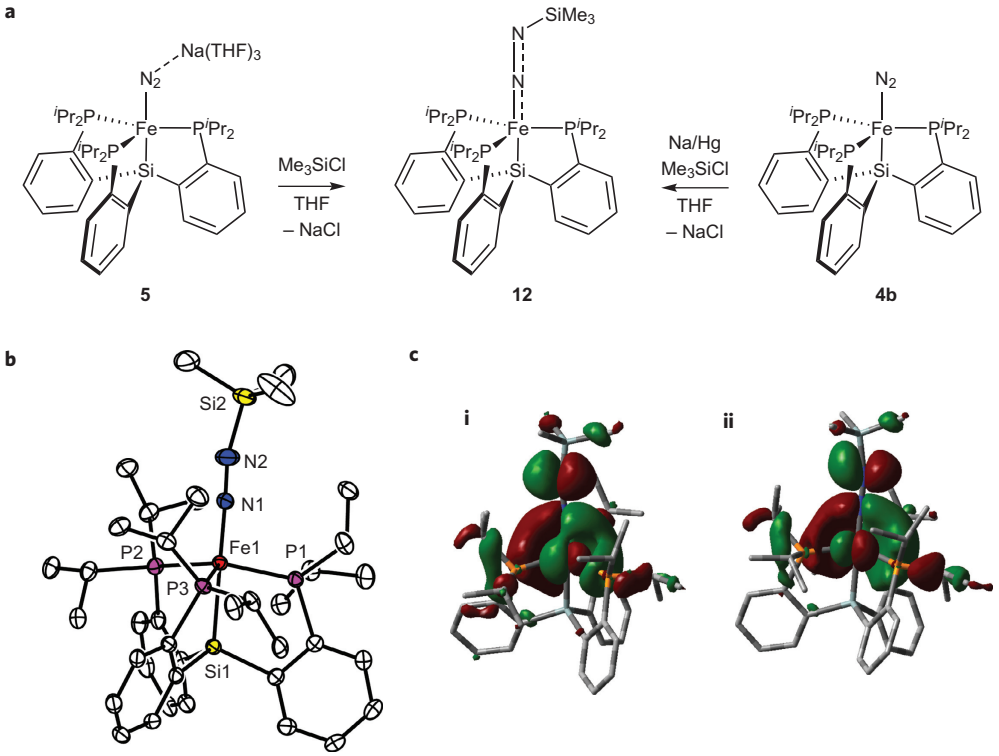

Figure 6 | Synthesis and characterization of 12. a, Synthesis of $(SiP^{i\text{-}Pr}{}_3)Fe(II)(N_2SiMe_3)$ (**12**) by silylation of **5** or by reductive silylation of **4b**. **b**, Solid-state structure of **12**. Hydrogen atoms are removed for clarity. Selected bond distances (Å) and angles (°) for **12**: Fe1–N1, 1.695(2); N1–N2, 1.195(3); Si2–N2, 1.720(3); Fe1–Si1, 2.3104(9); Fe1–P1, 2.2508(8); Fe1–P2, 2.2577(8); Fe1–P3, 2.2500(8); P1–Fe1–P2, 119.80(3); P2–Fe1–P3, 114.28(3); P3–Fe1–P1, 116.94(3); N1–Fe1–Si1, 175.78(9); N2–N1–Fe1, 175.7(3); N1–N2–Si2, 165.6(3). **c**, Density functional theory calculated highest occupied molecular orbital (HOMO) (**i**) and HOMO-1 (**ii**) of **12**. See Supplementary Information for details.

^{29}Si-NMR spectrum at 84.3 ppm (q, $^2J_{SiP} = 38$ Hz) and −15.6 ppm (s). A ^{15}N-NMR spectrum of the labelled complex ^{15}N-**12** shows two resonances at 418.5 and 270.9 ppm shifted from corresponding peaks for the ^{15}N-enriched precursor ^{15}N-**5** (340.3 and 309.7 ppm). From ^{29}Si-NMR measurements, ^{15}N–^{29}Si coupling was detected at −15.9 ppm (dd, $^{1,2}J_{SiN} = 10$, 2.2 Hz). However, no coupling was detected in the ^{31}P-NMR spectrum of the ^{15}N-enriched sample, even at −90 °C. Large separation between these two ^{15}N signals is fully consistent with functionalization at the dinitrogen ligand by the TMS group, as for the related molybdenum complex $(HIPTN_3N)$Mo–NNH species[42]. The ν(N–N) of **12** is 1,748 cm^{-1} (1,694 cm^{-1} for ^{15}N-**12**).

Dark-red crystals of **12** were obtained and an XRD analysis revealed a TMS group bound to N_β of the TBP iron scaffold ($\tau = 0.93$, Fig. 6). The relatively short Fe–N1 distance (1.695(2) Å) implies a multiple-bond character between the iron centre and N_α. The N–N bond distance of 1.195(3) Å establishes further reduction of the N_2 unit relative to its precursor **5** (1.147(4) Å), in which a Na^+ cation interacts with N_β. A single-point density functional theory calculation (Fig. 6, see Supplementary Information for details) of **12** illuminated the multiple-bond character between iron and N_α nicely, and revealed that the occupied molecular orbitals HOMO-2 and HOMO-3 possess significant π-bonding character between the Fe and N atoms. The difference in magnetic behaviour between diazenidos **10** and **12** is curious and is the subject of ongoing studies in our laboratory. We tentatively suggest that complex **12** is best formulated as a d^8 iron anion, akin to **5** and **5′**, that strongly backbonds into the $N_2SiMe_3{}^+$ π^* orbitals. Such a configuration for a TBP structure is expected to produce a diamagnet. By contrast, perhaps **10** is better formulated as a d^6 iron centre, which for a TBP structure provides a spin triplet in accordance with the numerous other $S = 1$ TBP iron(II) complexes described herein. The angle N_α–N_β–Si (165.6(3)°) for **12** is far less bent than the angle N_α–N_β–C in complex **10** (122.5(5)°), which is consistent with this comparative description.

To better evaluate the relative state of oxidation of the diamagnetic diazenido species **12** by comparison to the other $(SiP^{i\text{-}Pr}{}_3)Fe$ species described herein we collected Mössbauer spectra for solid samples of $(SiP^{i\text{-}Pr}{}_3)Fe(Cl)$, $(SiP^{i\text{-}Pr}{}_3)Fe(N_2)^+$ (**3**), $(SiP^{i\text{-}Pr}{}_3)Fe(N_2)$ (**4b**), $\{(SiP^{i\text{-}Pr}{}_3)Fe(N_2)\}\{Na(THF)_3\}$ (**5**), $\{(SiP^{i\text{-}Pr}{}_3)Fe(N_2)\}\{Na(12\text{-}C\text{-}4)_2\}$ (**5′**) and $(SiP^{i\text{-}Pr}{}_3)Fe(N_2SiMe_3)$ (**12**) in a zero external magnetic field at 77 K. Each of the spectra shows single quadrupole doublets (Fig. 7). Their isomer shifts (δ) and quadrupole splittings (E_Q) are listed in Fig. 7. The isomer shift of cationic **3** is very close to that of $(SiP^{i\text{-}Pr}{}_3)Fe(Cl)$ ($S = 1$) and consistent with those of other ferrous complexes[9]. The isomer shift decreases by about 0.1–0.15 mm s^{-1} per formal state of oxidation from **3** to **4b**, and from **4b** to **5** and **5′**. The isomer shift of the silyldiazenido species **12** is closer to that of **5** than **5′**, in accordance with our supposition that the TMS group that caps the N_2 ligand is electronically comparable to the $Na(THF)_3{}^+$ cation. Therefore, an Fe(0) d^8 assignment is best accorded to complex **12**, at least to the extent that such an assignment is appropriate for diamagnetic **5** and **5′**. As these complexes are highly covalent our primary intent here is to compare their relative states of oxidation with respect to one another.

In summary, the $\{(SiP^R{}_3)Fe\}$ scaffold continues to show its effectiveness in stabilizing nitrogenous donor ligands in the apical site of a TBP, *trans* to the silyl anchor of the ligand auxiliary. In particular, terminal N_2-binding is established structurally for the formal oxidation states Fe(0), Fe(I) and Fe(II). In addition, all of the five-coordinate iron(II) structures described herein are open-shell triplets. The synthesis of open-shell Fe–N_xH_y systems is of timely interest for comparison of their spectroscopic parameters with related data being obtained for the cofactor of nitrogenase under catalytic

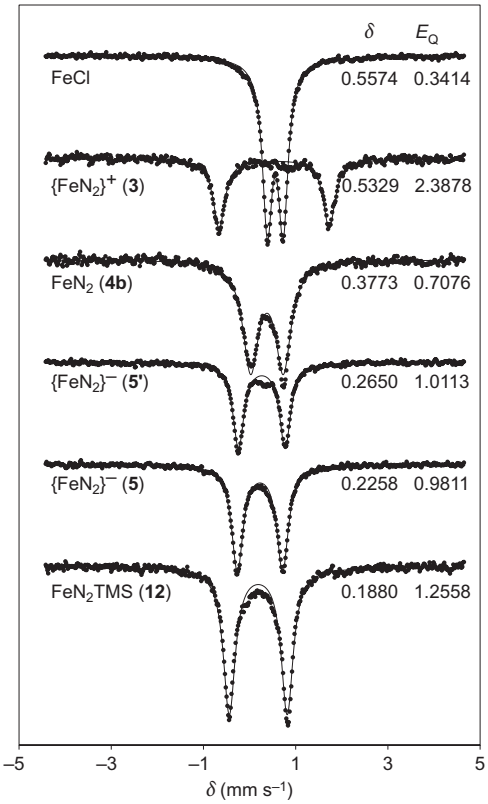

Figure 7 | Zero-field Mössbauer spectra. Spectra recorded at 77 K and offset from top to bottom in the order: $(SiP^{i\text{-}Pr}{}_3)Fe(Cl)$ (no effect with an applied external magnetic field of 45 mT was observed), $\{(SiP^{i\text{-}Pr}{}_3)Fe(N_2)\}\{B(ArF)_4\}$ (**3**), $(SiP^{i\text{-}Pr}{}_3)Fe(N_2)$ (**4b**), $\{(SiP^{i\text{-}Pr}{}_3)Fe(N_2)\}\{Na(12\text{-}C\text{-}4)_2\}$ (**5′**), $\{(SiP^{i\text{-}Pr}{}_3)Fe(N_2)\}\{Na(THF)_3\}$ (**5**) and $(SiP^{i\text{-}Pr}{}_3)Fe(N_2SiMe_3)$ (**12**). The dotted lines are the raw data and the solid lines are fits using the parameters listed.

turnover conditions[7,8]. The demonstration that the $\{(SiP^R{}_3)Fe\}$ scaffold can accommodate N_2, NH_3 and N_2H_4 in the apical site, and that $(SiP^R{}_3)Fe(II)–NH_3^+$ and $(SiP^R{}_3)Fe(II)–N_2H_4^+$ species can be recycled to give $(SiP^R{}_3)Fe(I)–N_2$ by chemical reduction with the concomitant liberation of NH_3, suggests to us that an iron-mediated, N_2-fixation catalyst system based on three-fold symmetry may yet be accessible. A promising lead is that the iron-bound N_2 ligand reacts with electrophiles at the Fe(0) state, which for the silyl derivatives afford stable $Fe–N_2SiR_3$ diazenido products.

Received 23 November 2009; accepted 29 March 2010; published online 16 May 2010

References

1. Saouma, C. T., Müller, P. & Peters, J. C. Characterization of structurally unusual diiron N_xH_y complexes. *J. Am. Chem. Soc.* **131,** 10358–10359 (2009).
2. Field, L. D., Li, H. L. & Magill, A. M. Base-mediated conversion of hydrazine to diazene and dinitrogen at an iron center. *Inorg. Chem.* **48,** 5–7 (2009).
3. Crossland, J. L., Balesdent, C. G. & Tyler, D. R. Intermediates in the reduction of N_2 to NH_3: synthesis of iron η^2 hydrazido(1-) and diazene complexes. *Dalton Trans.* 4420–4422 (2009).
4. Sellmann, D., Shaban, S. Y. & Heinemann, F. W. Syntheses, structures and reactivity of electron-rich Fe and Ru complexes with the new pentadentate ligand $Et_2NpyS_4–H_2$ {4-(diethylamino)-2,6-bis[(2-mercaptophenyl) thiomethyl]pyridine}. *Eur. J. Inorg. Chem.* 4591–4601 (2004).
5. Peters, J. C. & Mehn, M. P. *Activation of Small Molecules* Ch. 3 (Wiley, 2006).
6. Barney, B. M. *et al.* Diazene (HN = NH) is a substrate for nitrogenase: insights into the pathway of N_2 reduction. *Biochemistry* **46,** 6784–6794 (2007).
7. Barney, B. M. *et al.* A methyldiazene (HN = N–CH_3)-derived species bound to the nitrogenase active-site FeMo cofactor: implications for mechanism. *Proc. Natl Acad. Sci. USA* **103,** 17113–17118 (2006).
8. Barney, B. M. *et al.* Intermediates trapped during nitrogenase reduction of N≡N, CH_3−N=NH, and $H_2N–NH_2$. *J. Am. Chem. Soc.* **127,** 14960–14961 (2005).
9. Hendrich, M. P. *et al.* On the feasibility of N_2 fixation via a single site Fe^I/Fe^{IV} cycle–spectroscopic studies of $Fe^I(N_2)Fe^I$, Fe^{IV}≡N, and related species. *Proc. Natl Acad. Sci. USA* **103,** 17107–17112 (2006).
10. MacBeth, C. E., Harkins, S. B. & Peters, J. C. Synthesis and characterization of cationic iron complexes supported by the neutral ligands $NP^{i\text{-}Pr}{}_3$, $NArP^{i\text{-}Pr}{}_3$, and $NS^{t\text{-}Bu}{}_3$. *Can. J. Chem.* **83,** 332–340 (2005).
11. Hinnemann, B. & Nørskov, J. K., Modeling a central ligand in the nitrogenase FeMo cofactor. *J. Am. Chem. Soc.* **125,** 1466–1467 (2003).
12. Mankad, N. P., Whited, M. T. & Peters, J. C. Terminal $Fe^I–N_2$ and Fe(II) · · · H–C interactions supported by tris(phosphino)silyl ligands. *Angew. Chem. Int. Ed.* **46,** 5768–5771 (2007).
13. Whited, M. T., Mankad, N. P., Lee, Y., Oblad, P. F. & Peters, J. C. Dinitrogen complexes supported by tris(phosphino)silyl ligands. *Inorg. Chem.* **48,** 2507–2517 (2009).
14. Bowman, A. C. *et al.* Synthesis and molecular and electronic structures of reduced bis(imino)pyridine cobalt dinitrogen complexes: ligand versus metal reduction. *J. Am. Chem. Soc.* **132,** 1676–1684 (2010).
15. Betley, T. A. & Peters, J. C. Dinitrogen chemistry from trigonally coordinated iron and cobalt platforms. *J. Am. Chem. Soc.* **125,** 10782–10783 (2003).
16. Addison, A. W., Rao, T. N., Reedijk, J., van Rijn, J. & Verschoor, G. C. Synthesis, structure and spectroscopic properties of copper(II) compounds containing nitrogen–sulfur donor ligands; the crystal and molecular structure of aqua[1,7-bis(*N*-methylbenzimidazol-2′-yl)-2,6-dithiaheptane]copper(II) perchlorate. *J. Chem. Soc. Dalton Trans.* 1349–1356 (1984).
17. Yandulov, D. V. & Schrock, R. R. Studies relevant to catalytic reduction of dinitrogen to ammonia by molybdenum triamidoamine complexes. *Inorg. Chem.* **44,** 1103–1117 (2005).
18. Field, L. D., Li, H. L., Dalgarno, S. J. & Turner, P. The first side-on bound metal complex of diazene, HN=NH. *Chem. Commun.* 1680–1682 (2008).
19. Crossland, J. L., Zakharov, L. N. & Tyler, D. R. Synthesis and characterization of an iron(II) η^2-hydrazine complex. *Inorg. Chem.* **46,** 10476–10478 (2007).
20. Yu, Y., Brennessel, W. W. & Holland, P. L. Borane B–C bond cleavage by a low-coordinate iron hydride complex and N–N bond cleavage by the hydridoborate product. *Organometallics* **26,** 3217–3226 (2007).
21. Shakir, M., Parveen, S., Begum, N. & Azim, Y. Interaction of manganese(II), iron(II), cobalt(II), nickel(II), copper(II) and zinc(II) with acetylhydrazine, formed *in situ*; first crystal structure of tris(acetylhydrazine) nickel(II) perchlorate. *Trans. Metal Chem.* **29,** 916–920 (2004).
22. Albertin, G., Antoniutti, S., Bordignon, E. & Chimisso, F. Preparation of bis(hydrazine) complexes of iron(II). *Inorg. Chem. Commun.* **4,** 402–404 (2001).
23. Sellmann, D., Soglowek, W., Knoch, F., Ritter, G. & Dengler, J. Transition-metal complexes with sulfur ligands. 88. Dependence of spin state, structure, and reactivity of [Fe(II)(L)('N_HS_4')] complexes on the coligand L (L = CO, N_2H_2, N_2H_4, NH_3, pyridine, $NHCH_3NH_2$, CH_3OH, THF, $P(OCH_3)_3$, $P(OPh)_3$): model complexes for iron nitrogenases ('N_2H_4'$^{2-}$ = dianion of 2,2′-bis[(2-mercaptophenyl)thio]diethylamine). *Inorg. Chem.* **31,** 3711–3717 (1992).
24. Casey, M. T. *et al.* Reaction of 1,1′-diacetylferrocene with hydrazine hydrate: synthesis and X-ray crystal structures of bis(hydrazine)bis(hydrazinecarboxylato-N′,O)iron(II), $[Fe(N_2H_4)_2(O_2CNHNH_2)_2]$, and the cyclic biferrocene diazine, $[—N(Me)CC_5H_4FeC_5H_4C(Me)N—]_2$. *Polyhedron* **10,** 483–489 (1991).
25. Goedken, V. L., Peng, S.-M., Molin-Norris, J. & Park, Y.-A. Carbon monoxide complexes of iron(II): synthesis and structural studies of five- and six-coordinate complexes of the macrocyclic ligand, $C_{22}H_{22}N_4^{2-}$. *J. Am. Chem. Soc.* **98,** 8391–8400 (1976).
26. Davies, S. C. *et al.* Vanadium complexes of the $N(CH_2CH_2S)_3^{3-}$ and $O(CH_2CH_2S)_2^{2-}$ ligands with coligands relevant to nitrogen fixation processes. *Inorg. Chem.* **39,** 3485–3498 (2000).
27. Alhomaidan, O., Hollink, E. & Stephan, D. W. Main group heterocycles from lithiated phosphinimines. *Organometallics* **26,** 3041–3048 (2007).
28. Aguilar, D., Contel, M., Navarro, R. & Urriolabeitia, E. P. Organogold(II) iminophosphorane complexes as efficient catalysts in the addition of 2-methylfuran and electron-rich arenes to methyl vinyl ketone. *Organometallics* **26,** 4604–4611 (2007).
29. Bielsa, R., Larrea, A., Navarro, R., Soler, T. & Urriolabeitia, E. P. Synthesis, structure, reactivity, and catalytic activity of *C,N,N*- and *C,N,N*-orthopalladated iminophosphoranes. *Eur. J. Inorg. Chem.* 1724–1736 (2005).
30. Chan, K. T. K. *et al.* Anionic phosphinimine-chelate complexes of rhodium and iridium: steric and electronic influences on oxidative addition of CH_2Cl_2. *Organometallics* **23,** 381–390 (2004).
31. Spencer, L. P. *et al.* Pyridine– and imidazole–phosphinimine bidentate ligand complexes: considerations for ethylene oligomerization catalysts. *Organometallics* **22,** 3841–3854 (2003).
32. LePichon, L., Stephan, D. W., Gao, Z. & Wang, Q. Iron phosphinimide and phosphinimine complexes: catalyst precursors for ethylene polymerization. *Organometallics* **21,** 1362–1366 (2002).

33. Mountford, A. J. *et al*. Intra- and intermolecular N–H · · · F–C hydrogen-bonding interactions in amine adducts of tris(pentafluorophenyl)borane and -alane. *Inorg. Chem.* **44,** 5921–5933 (2005).
34. Hyla-Kryspin, I., Haufe, G. & Grimme, S. Weak hydrogen bridges: a systematic theoretical study on the nature and strength of C–H · · · F–C interactions. *Chem. Eur. J.* **10,** 3411–3422 (2004).
35. Brammer, L., Bruton, E. A. & Sherwood, P. Understanding the behavior of halogens as hydrogen bond acceptors. *Cryst. Growth Des.* **1,** 277–290 (2001).
36. Takemura, H. *et al*. The C–F · · · cation interaction: an ammonium complex of a hexafluoro macrocyclic cage compound. *Chem. Eur. J.* **6,** 2334 (2000).
37. Howard, J. A. K., Hoy, V. J., O'Hagan, D. & Smith, G. T. How good is fluorine as a hydrogen bond acceptor? *Tetrahedron* **52,** 12613–12622 (1996).
38. Davies, S. C., Hughes, D. L., Richards, R. L. & Sanders, J. R. Molybdenum and tungsten complexes of the $N(CH_2CH_2S)_3^{3-}$ (NS_3) ligand with oxide, sulfide, diazenide, hydrazide and nitrosyl co-ligands. *J. Chem. Soc. Dalton Trans.* 719–725 (2000).
39. Albertin, G. *et al*. Reactivity of hydrides $FeH_2(CO)_2P_2$ (P = phosphites) with aryldiazonium cations: preparation, characterization, X-ray crystal structure, and electrochemical studies of mono- and binuclear aryldiazenido complexes. *Inorg. Chem.* **37,** 5602–5610 (1998).
40. Albertin, G., Antoniutti, S., Pelizzi, G., Vitali, F. & Bordignon, E. Bis(aryldiazene) derivatives of iron(II): preparation, characterization, and properties of the first complexes containing two diazene ligands bonded to the same central metal. The X-ray crystal structures of hexacoordinate $[FeH(4\text{-}CH_3C_6H_4NNH)[P(OEt)_3]_4]^+$, and pentacoordinate $[Fe(4\text{-}CH_3C_6H_4N_2)[P(OEt)_3]_4]^+$ cations. *J. Am. Chem. Soc.* **108,** 6627–6634 (1986).
41. Haymore, B. L. & Ibers, J. A. Aryldiazo complexes. Structure of an iron–aryldiazo complex, dicarbonyl bis(triphenylphosphine) benzenediazonium iron(1+) tetrafluoroborate (1–). *Inorg. Chem.* **14,** 1369–1376 (1975).
42. Yandulov, D. V. & Schrock, R. R. Reduction of dinitrogen to ammonia at a well-protected reaction site in a molybdenum triamidoamine complex. *J. Am. Chem. Soc.* **124,** 6252–6253 (2002).

Acknowledgements

We acknowledge the National Institutes of Health (GM-070757). Funding for the Massechussetts Institute of Technology Department of Chemistry Instrumentation Facility was provided in part by the National Science Foundation (NSF) (CHE-0234877). P. Mueller provided assistance with XRD analyses. N.P.M. received an NSF graduate fellowship. We thank R.H. Holm and T.A. Betley at Harvard University for providing us with access to a Mössbauer spectrometer.

Author contributions

Y.L., N.P.M. and J.C.P. conceived and designed the experiments, Y.L. and N.P.M. performed the experiments and Y.L. and J.C.P. co-wrote the paper.

Additional information

The authors declare no competing financial interests. Supplementary information and chemical compound information accompany this paper at www.nature.com/naturechemistry. Reprints and permission information is available online at http://npg.nature.com/reprintsandpermissions/. Correspondence and requests for materials should be addressed to J.C.P.